Original Research

Atorvastatin Calcium Enhances Ferroptosis in Breast Cancer Cells Through Mechanisms Involving DECR1

Yao Li[1,2], Hongdan Chen[2,3], Zeyu Yang[2], Yinde Huang[2], Fan Zhang[2,*] , Huaizhi Wang[1,4,5,*]

[1]Graduate School of Medicine, Chongqing Medical University, 400016 Chongqing, China
[2]Department of Breast and Thyroid Surgery, Chongqing General Hospital, Chongqing University, 401147 Chongqing, China
[3]College of Pharmaceutical Sciences & College of Chinese Medicine, Southwest University, 400715 Chongqing, China
[4]Institute of Hepatopancreatobiliary Surgery, Chongqing General Hospital, Chongqing University, 401147 Chongqing, China
[5]Chongqing Key Laboratory of Intelligent Medicine Engineering for Hepatopancreatobiliary Diseases, 401147 Chongqing, China
*Correspondence: zhangfancgh@163.com (Fan Zhang); whuaizhi@gmail.com (Huaizhi Wang)
Academic Editor: Jordi Sastre-Serra
Submitted: 10 March 2025   Revised: 25 April 2025   Accepted: 22 May 2025   Published: 26 June 2025

Abstract

Background: Breast cancer is currently the most prevalent malignancy among females, representing a substantial threat to both physical and psychological health. Moreover, its incidence rate continues to rise annually. Therefore, screening potential therapeutic targets and developing candidate drugs for breast cancer treatment holds significant clinical implications. **Methods**: In this study, *in silico* methods were used to identify potential therapeutic targets of fatty acid metabolism-related genes in breast cancer and to screen potential drugs using molecular docking. In addition, Cell Counting Kit-8 (CCK-8) and Transwell assays were utilized to analyze the effect of atorvastatin calcium (AC) on the malignant phenotype of breast cancer cells. Furthermore, the effects of AC-induced ferroptosis in tumor cells were evaluated using transmission electron microscopy, ROS, Fe^{2+}, and Liperfluo probes, and the potential molecular mechanisms were explored through real-time qPCRand western blotting. **Results**: 2,4-Dienoyl-CoA Reductase 1 (DECR1) overexpression was related to a dismal prognostic outcome in breast cancer patients. AC interfered with breast cancer cell proliferation and invasion, potentially through its effects in DECR1 expression, while suppressing tumor growth *in vivo*. In addition, AC demonstrated antitumor effects, possibly through the downregulation of DECR1 and the upregulation of Acyl-CoA Synthetase Long-Chain Family Member 4 (ACSL4), which may contribute to the induction of ferroptosis in tumor cells. **Conclusions**: DECR1 is associated with breast cancer progression and may serve as a potential therapeutic indicator, and AC plays an antitumor role by modulating DECR1 expression and promoting ACSL4-mediated ferroptosis. Therefore, AC may be considered a potential candidate drug for treating breast cancer.

Keywords: breast cancer; DECR1; atorvastatin calcium; ferroptosis

1. Introduction

Breast cancer (BC), a female cancer with a high prevalence, greatly threatens female health. Ferroptosis is programmed cell death characterized by iron-dependent lipid peroxide accumulation. The accumulation of lipid ROS and reduced antioxidant ability of cells ultimately cause ferroptosis. In BC, ferroptosis disrupts various cell metabolic pathways, including lipid and amino acid metabolism, and also the redox homeostasis [1]. Ferroptosis affects multiple aspects of BC, such as tumor invasion and metastasis [2], stemness [3], and drug resistance [4] indicating its potential for use in a viable intervention strategy.

Statins can inhibit 3-Hydroxy-3-Methylglutaryl-Coenzyme A (HMG-CoA) reductase in the mevalonate pathway to decrease blood cholesterol. Clinically, statins have been used mainly to treat hyperlipidemia, atherosclerosis, and other diseases related to lipid metabolism. Rapidly proliferating cells require cholesterol in huge amounts for cell membrane synthesis, which suggests that statins could reduce the level of low-density lipoprotein

and the secretion of proinflammatory factors. The role of statins in tumors has been widely studied. Statins reportedly reduce BC recurrence and mortality. The currently known statins may suppress solid cancers such as prostate, liver, and gastric cancers [5,6].

A previous study reported that simvastatin induced BC cell ferroptosis by downregulating Glutathione Peroxidase 4 (GPX4) and inactivating the mevalonate pathway [7]. Another study reported that statins exhibit antitumor activity by degrading the mutated P53 protein and promoting cell cycle arrest to induce cell apoptosis [8]. The therapeutic potential of statins in tumors has been confirmed; however, the role of atorvastatin calcium in inhibiting tumor growth in BC through the induction of ferroptosis and the related mechanisms have not yet been elucidated.

Acyl-coenzyme A synthase long-chain family member 4 (ACSL4) has been proven to be one of the key driving factors of ferroptosis. ACSL4 is a key isoenzyme that is related to the biological metabolism of polyunsaturated fatty acids (PUFAs), determining the sensitivity of the latter to ferroptosis. ACSL4 connects coenzyme A with

long-chain PUFAs and then exchanges them with phospholipids through lysophosphatidylcholine acyltransferase, thereby promoting the integration of long-chain polyunsaturated fatty acids with lipids and membranes. ACSL4 upregulation enhances ferroptosis sensitivity in cells through the optimization of PUFA catalysis. Therefore, activating ACSL4-dependent pathway is considered a key strategy to increase the sensitivity of cancer cells to ferroptosis [9].

The results of the present study suggested that 2,4-Dienoyl-CoA Reductase 1 (DECR1) has an important effect on BC development and that atorvastatin calcium (AC) induces ferroptosis by targeting the DECR1-ACSL4 axis. These findings highlighted the potential of AC as a candidate drug for treating BC, providing a strategy to combat this prevalent cancer.

2. Materials and Methods

2.1 Bioinformatics Analysis

The Cancer Genome Atlas (TCGA-BRCA) contains the data of 1109 BC and 113 non-carcinoma breast samples. The Molecular Taxonomy of Breast Cancer International Consortium (METABRIC) has the data of 1904 BC samples, whereas the Gene Expression Omnibus (GEO) database, specifically the GSE96058 dataset, includes the data of 3409 BC samples. The Molecular Signatures Database (MSigDB) v7.4 was adopted in this study to identify the fatty acid metabolism genes, including those related to the KEGG fatty acid metabolism pathway, Reactome fatty acid metabolism, and hallmarks of fatty acid metabolism [10,11]. The overlapping genes were removed from these identified genes, and 309 fatty acid metabolism-related genes (FMGs) remained. Subsequently, these 309 FMGs were intersected with the total genes from the TCGA-BRCA, METABRIC, and GSE96058 datasets, and 269 reliable FMGs were identified and used for further analysis.

Weighted gene coexpression network analysis (WGCNA) is a systems biology method used to describe the patterns of gene associations across different samples [12]. Using the imageGP website (https://www.bic.ac.cn), a WGCNA was conducted in this study for the expression data of the above-identified 269 FMG genes in cancer and tumor tissues from the TCGA-BRCA dataset, and the gene adjacency heatmaps were obtained. Next, univariate Cox analysis was conducted to identify the correlations of the genes in the module most associated with tumors to the overall survival rate in the TCGA-BRCA cohort, with an objective of identifying the hub genes related to fatty acid metabolism ($p < 0.05$ indicated statistical significance).

Thereafter, the DECR1 protein levels in tumor and matched non-carcinoma tissues were determined from the Human Protein Atlas (HPA) database (https://www.proteinatlas.org/). Immunohistochemical (IHC) staining was semi-quantitatively scored by multiplying staining intensity (0–3) with the percentage of positive cells (1–4), yielding a total score ranging from 0 to 12. Intensity was graded as: 0 = negative, 1 = weak, 2 = moderate, 3 = strong. Proportion scores were: 1 = ≤25%, 2 = 26–50%, 3 = 51–75%, 4 = >75%. The percentage of positively stained cells was also scored on a 4-point scale: 1 = ≤25%, 2 = 26–50%, 3 = 51–75%, 4 = >75%. The final IHC score was calculated by multiplying the intensity score by the proportion score, yielding a composite score ranging from 0 to 12. Furthermore, the relationship between DECR1 and overall survival in patients with breast cancer was investigated using the Kaplan-Meier Plotter database (https://kmplot.com/analysis/). The Tumor and Immune System Interaction Database (TISIDB) database [13] was used to analyze the relationships of DECR1 with breast cancer immune subtypes and breast cancer subtypes. The immune subtypes were identified as C1–C6 according to the criteria reported by Thorsson *et al.* [14].

2.2 Drug Screening

The natural product library of TargetMol (TargetMol, Boston, MA, USA), which contains the data of about 19,000 natural small-molecule compounds, was used for drug screening. All compounds were docked to the binding port defined by the DECR1 protein (ID: 1W6U) using a three-step method. High-throughput screening was completed in step 1, retaining 50% of the compounds; standard precision was performed in step 2, and 50% of the compounds from the previous step were retained; extra precision was conducted in step 3, in which, 50% of the compounds from step 2 were retained. By setting the compound properties to 0 < H bond donor < 6 and 150 < Mol weight < 725, the compounds were further screened, revealing 1258 compounds after screening.

2.3 Molecular Docking

These 1258 compounds were zipped and input into Canvas to calculate the binary fingerprints of all small molecules. Then, hierarchical clustering was performed on the Tanimoto similarity matrix. From each class, the docking score (in kcal/mol, where a smaller value represents the highest affinity between the receptor and ligand) was selected, and the highest number of small-molecule compounds was retained. Finally, 100 small molecule compounds belonging to different chemical structures were obtained. An intersection analysis between these 100 obtained small molecule compounds and the drugs already listed in the Food and Drug Administration (FDA) database was performed, revealing two drugs: atorvastatin calcium and pravastatin sodium. The ligands pravastatin and atorvastatin, along with the DECR1 protein (1W6U), were subsequently submitted to SwissDock (http://www.swissdock.ch) for molecular docking using AutoDock Vina (The Scripps Research Institute, La Jolla, CA, USA) [15,16]. Finally, Proteins Plus (https://proteins.plus/) was used for visualization and processing, and images were obtained.

2.4 Surface Plasmon Resonance (SPR)

This experiment was conducted in accordance with the standard Surface Plasmon Resonance (SPR)-related procedures. The experimental design and parameters are shown in the table below. In brief, the carboxyl (COOH) chip was installed on the OpenSPRTM instrument (Nicoya Lifesciences, Kitchener, ON, Canada), the sample ring was cleaned with PBS buffer, and the chip was activated with 1-Ethyl-3-(3-dimethylaminopropyl)carbodiimide/N-Hydroxysuccinimide (EDC/NHS, 1:1) solution when the signal reached the baseline. The DECR1 ligand (200 µL) was loaded followed by incubation for 4 min. The analyte was diluted with buffer (PBS + 1% DMSO) and loaded at a rate of 20 µL/min. The protein and ligand binding time were 240 s, and natural dissociation was allowed for 300 s. Data analysis was performed using the one-to-one analysis model in TraceDrawer (Ridgeview Instruments AB, Uppsala, Sweden) software.

2.5 Cell Culture

The BC cell lines BT474, MDA-MB-231, and 4T1 were purchased from ATCC (American Type Culture Collection, Manassas, VA, USA). BT474 and MDA-MB-231 cells were cultured in Dulbecco's modified Eagle's medium (DMEM) (SH30022.01B, HyClone, Logan, UT, USA) supplemented with 10% fetal bovine serum (SH30088.03, HyClone, Logan, UT, USA), 100 U/mL penicillin, and 100 µg/mL streptomycin (C0222, Beyotime, Suzhou, Jiangsu, China), and 4T1 cells were cultured in RPMI-1640 (SH30809.01B, HyClone, Logan, UT, USA) complete medium. All cells were incubated at 37 °C in 5% CO_2 for culture, and the medium was changed every 2–3 days. All cell lines used in this study were validated by Short Tandem Repeat (STR) profiling and tested negative for mycoplasma contamination.

2.6 Cell Proliferation Assay

The logarithmic BC cells were seeded and cultured in the wells of 96-well plates overnight, followed by further seeding and culture in the medium containing atorvastatin calcium (T3116, TargetMol, Boston, MA, USA) or pravastatin sodium (T0672, TargetMol, Boston, MA, USA) for 48 h at 37 °C with 5% CO_2. The cell seeding concentrations used were 0, 3.125, 6.25, 12.5, 25, 50, 100, and 200 µM. After 48 h of cell culture, the breast cancer cells were treated with the CCK-8 solution (BS350B, Biosharp, Hefei, Anhui, China), and absorbance values were read at 450 nm.

2.7 Cell Migration

DMEM (with 10% FBS) and breast cancer cells were added to the top Transwell chamber (3464, Corning, Corning, NY, USA), and only DMEM (with 20% FBS) was added to the bottom chamber. At 48 h of incubation at 37 °C, 0.1% crystal violet was added for cell staining, followed by microscopic observation and cell counting.

2.8 Transmission Electron Microscopy

The cells from the different treatment groups (1500 rpm, 5 min) were centrifuged, and the cells were collected in centrifuge tubes. The samples were fixed with 3% pentanediol and then with 1% osmium tetroxide, followed by dehydration with gradient acetone and embedding in the Epon-812 embedding agent. An ultrathin slicing mechanism (Leica Microsystems, Wetzlar, Hesse, Germany) was used to prepare ultrathin slices of about 60–90 nm, and a JEM-1400FLASH transmission electron microscope (JEOL Ltd., Tokyo, Japan) was used to acquire images of these slices when observed.

2.9 ROS, Fe^{2+}, and Lipid Peroxide Levels

A DCFH-DA probe (Beyotime, China, S0033M) was used to evaluate the intracellular ROS levels. A FerroOrange probe (F374, Dojindo Laboratories, Kumamoto, Japan) was used to detect the intracellular Fe^{2+} content. A Liperfluo assay kit (DOJINDO, Japan, L248) was used to measure the levels of lipid peroxides. Each experiment was performed following specific protocols, and a fluorescence microscope (Leica Microsystems, Wetzlar, Hesse, Germany) was used for observation.

2.10 Real-time qPCR

The total RNA in the samples was extracted with TRIzol Reagent (15596026, Invitrogen, Carlsbad, CA, USA) and then reverse transcribed into cDNA using the HiScript II Q RT SuperMix for qPCR Reagent Kit (R223-01, Vazyme, Nanjing, Jiangsu, China). The RT-PCR system was configured using ChamQ Universal SYBR qPCR Master Mix (Q711-02, Vazyme, Nanjing, Jiangsu, China), and the primer sequences used for qPCR are listed in Table 1. The amplification reactions were performed using a real-time qPCR instrument (Archimed-X6, ROCGENE, Wuhan, Hubei, China). Gene expression was calculated using the $2^{-\Delta\Delta ct}$ approach, with GAPDH used as an endogenous reference. The primers used were as in Table 1.

2.11 Western Blotting

Radioimmunoprecipitation assay (RIPA) lysis buffer supplemented with a protease inhibitor cocktail was used for cell lysis. A BCA kit (P0012, Beyotime, Suzhou, Jiangsu, China) was used to determine the protein content. Protein aliquots were then subjected to western blotting. The following primary antibodies were used: anti-β-actin (ab6276, Abcam, Cambridge, Cambridgeshire, UK), anti-DECR1 (ab198848, Abcam, Cambridge, Cambridgeshire, UK), and anti-ACSL4 (sc-365230, Santa Cruz Biotechnology, Dallas, TX, USA). HRP-conjugated secondary antibodies (SA00001-1 and SA00001-2, Proteintech, Chicago, IL, USA) were utilized to detect the bound antibodies using an enhanced chemiluminescence (ECL) kit (P0018S, Beyotime, Suzhou, Jiangsu, China).

Table 1. Primer sequences used for real-time qPCR.

Gene Symbol	Sequence (5′–3′)
NCOA4	F: GAGGTGTAGTGATGCACGGAG
	R: GACGGCTTATGCAACTGTGAA
NRF2	F: TCAGCGACGGAAAGAGTATGA
	R: CCACTGGTTTCTGACTGGATGT
GPX4	F: GAGGCAAGACCGAAGTAAACTAC
	R: CCGAACTGGTTACACGGGAA
DECR1	F: TCTTCAAAAAGCGATGCTACCA
	R: CTATCACGCACTGAGCACCT
FTH1	F: TCCTACGTTTACCTGTCCATGT
	R: GTTTGTGCAGTTCCAGTAGTGA
SLC7A11	F: TCTCCAAAGGAGGTTACCTGC
	R: AGACTCCCCTCAGTAAAGTGAC
KEAP1	F: CTGGAGGATCATACCAAGCAGG
	R: GGATACCCTCAATGGACACCAC
P53	F: CAGCACATGACGGAGGTTGT
	R: TCATCCAAATACTCCACACGC
ACSL4	F: AACCCAGAAAACTTGGGCATT
	R: GTCGGCCAGTAGAACCACT
GAPDH	F: GGAGCGAGATCCCTCCAAAAT
	R: GGCTGTTGTCATACTTCTCATGG

2.12 Animal Experiments

Female BALB/c mice (about 6 weeks old) were procured from Hunan SJA Laboratory Animal Co., Ltd. (Changsha, Hunan, China). The experimental animals were raised at the experimental animal center of Southwest University under specific pathogen-free conditions. The purchase, shipping, housing, care, and euthanization of all mice were in accordance with the guidelines of the Institutional Animal Care and Use Committee of Southwest University.

The 100 µL of a 4T1 breast cancer cell suspension with 1×10^6 cells were injected subcutaneously into the axillary region of BALB/c mice to construct the subcutaneous breast cancer xenograft model. At a volume of about 50 mm^3, atorvastatin calcium (20 mg/kg and 40 mg/kg) were administered intraperitoneally, once every 2 days, for 6 times. The tumor volume was then calculated as follows: volume = (length × width^2)/2 at 2-day intervals where length refers to the longest dimension and width refers to the perpendicular shorter axis. To ensure accuracy, all measurements were performed using digital calipers by trained personnel in a blinded manner, and tumors with irregular morphology or poorly defined boundaries were excluded from volumetric analysis. After receiving six doses of the treatment, the mice were euthanized for further analysis and the required tissue samples were retrieved. All animals were euthanized humanely using carbon dioxide (CO$_2$) inhalation, with a fill rate of 20% chamber volume per minute, in accordance with the AVMA Guidelines (2020) and approved by the Institutional Animal Care and Use Committee (IACUC).

2.13 HE and Immunohistochemical Staining Analyses

Mouse tumor, liver, kidney, and spleen samples were collected and immersed in 4% paraformaldehyde at ambient temperature. The paraffin-embedded samples were later sliced into 5 µm sections for hematoxylin-eosin (H&E) staining.

After 24 h of immersion in 10% neutral formalin, the tumor tissues were subjected to paraffin embedding and then sliced into 5 µm sections. Afterward, the sections were deparaffinized and rehydrated, followed by antigen retrieval by boiling in citrate buffer (pH 6.0) for 15 min. Thereafter, 3% hydrogen peroxide was added to block the endogenous peroxide for 10 min. The sections were blocked with 5% goat serum for 1 h and then incubated overnight at 4 °C with DECR1 antibody (Abcam, England, ab198848) and Ki67 antibody (Abcam, England, ab15580). The sections were then washed followed by 1 h of incubation with an HRP-labeled secondary antibody and then 3,3′-Diaminobenzidine (DAB) staining for 5 min. Hematoxylin was used for counterstaining, and the slides were dehydrated, cleared, and mounted. Images of the sections were captured using a microscope (Leica Microsystems, Wetzlar, Hesse, Germany).

2.14 Statistical Analysis

The results were presented as means ± standard deviations (SDs). Intra-group differences were compared using the Student's t-test, whereas inter-group differences were analyzed using one-way ANOVA. Every assay was conducted at least three times. $p < 0.05$ indicated statistical sig-

nificance. GraphPad Prism 9.0 software (GraphPad Software, San Diego, CA, USA) was used for statistical analysis.

3. Results

3.1 DECR1 Could Be a Candidate Anti-BC Therapeutic Target

The effects of the reprogramming of fatty acid metabolism on BC occurrence and development are undeniable. Therefore, the genes associated with fatty acid metabolism were screened to identify tumor therapeutic targets. The fatty acid metabolism-related genes associated with BC were identified from the TCGA-BRCA (n = 1109), METABRIC (n = 1904), and GSE96058 (n = 3409) datasets, and the intersection revealed 269 potential genes (**Supplementary Table 1**, Fig. 1A). Subsequently, WGCNA was performed for these 269 genes to identify the module most strongly associated with tumors. WGCNA revealed a positive correlation between the brown module and the tumor phenotype (R = 0.334, $p < 0.0001$) (Fig. 1B,C), and 50 genes from this module were selected for subsequent analysis (**Supplementary Table 2**) using a univariate Cox analysis. DECR1 was consequently identified as a risk factor for breast cancer, whereas PTGS2, ALDH3A1, PLA2G4A, ALDH2, ACSL5, and CYP1B1 were identified as protective factors (Fig. 1D). Subsequent analysis focused on determining the role of DECR1 in breast cancer.

3.2 DECR1 Expression Can Predict Poor Prognosis in Breast Cancer Patients

Compared to its levels in the adjacent tissues, DECR1 was significantly overexpressed in breast cancer tissues (Fig. 1E). Next, based on the average expression of DECR1 in TCGA-derived breast cancer tissues, the patients were classified into DECR1 low-expression or DECR1 high-expression groups using a cutoff of 50%. DECR1 exhibited significant differential expression in BRCA (Kruskal-Wallis test, $p = 9.46 \times 10^{-7}$), potentially associated with cluster groups (C1–C6) or distinct molecular subtypes (e.g., Basal-like, HER2, Luminal) (Fig. 1G,H). According to the survival analysis, high DECR1 expression was negatively correlated to patient prognosis (Fig. 1F), indicating that high DECR1 expression was associated with poor outcomes. These results suggested that DECR1 is closely associated with BC prognosis, although the underlying mechanisms remain unclear.

3.3 Atorvastatin Calcium Exerts Antitumor Effects Associated With DECR1 in Breast Cancer

The preliminary research showed that DECR1 could serve as a prognostic indicator with a negative correlation to patient prognosis. Therefore, searching for potential candidate drugs targeting DECR1 has clinical significance and prospects. Accordingly, computer-aided screening was conducted in this, for which the ligand NADP in

the DECR1 complex structure (Fig. 2A) was defined as the binding pocket and the top 100 compounds screened were intersected with the FDA-marketed drug database. As a result, atorvastatin calcium (AC) and pravastatin sodium (Fig. 2B,C), which could bind to the DECR1 protein, were identified. AC formed hydrogen bonds with the DECR1 protein at Thr69, Gly72, Ala146, Phe249, and Asn144. Additionally, the Phe249 and Leu71 residues were involved in hydrophobic interactions (Fig. 2D). Pravastatin sodium formed hydrogen bonds at Tyr199, Ile243, Thr245, Gly147, and Ser210, while hydrophobic interactions were noted with Thr197 and Leu71 (Fig. 2E). To investigate the direct interaction between DECR1 and atorvastatin calcium (AC), surface plasmon resonance (SPR) analysis was performed (Fig. 2F). A concentration-dependent binding curve demonstrated that AC binds to DECR1 with high affinity and specificity *in vitro*.

Furthermore, the effects of AC and PS on BC cell proliferation were evaluated, and it was confirmed that AC could suppress MDA-MB-231 and BT474 cell growth, with IC50 values of 39.70 μM and 7.74 μM, respectively (Fig. 3A,B). However, BC cells are insensitive to different concentrations of pravastatin sodium; therefore, it was speculated that AC has greater potential than pravastatin sodium to efficiently treat BC. Therefore, further research was conducted using AC. BC cell migration ability was markedly inhibited following AC treatment (Fig. 3C,D). The *in vivo* research revealed that AC administration significantly inhibited tumor development (Fig. 4A,B), and a preliminary *in vivo* safety assessment revealed that AC caused little harm to key organs in the tumor burden model, as evidenced by HE staining showing no significant morphological changes in the liver, kidney, or spleen. Additionally, immunohistochemical staining of tumor tissues demonstrated a marked decrease in Ki67 and DECR1 expression after AC treatment, indicating suppressed tumor cell proliferation and downregulation of DECR1 in *vivo* (Fig. 4C,D). In summary, our findings suggest that the antitumor effect of AC may be linked to its regulation of DECR1.

3.4 Atorvastatin Calcium Inhibits Cell Survival by Inducing Ferroptosis in Breast Cancer Cells

Clinically, AC is used mainly to treat hyperlipidemia, atherosclerosis, and other lipid metabolism disorders. Accordingly, combined with the findings of this study, it was speculated that the potential role of AC is to affect fat metabolism in cells. Statins have been suggested to induce ferroptosis in different solid cancers by inhibiting the mevalonate pathway to reduce the biosynthesis of GPX4. Therefore, whether AC could induce ferroptosis in breast cancer cells was evaluated next in this study. Transmission electron microscopy revealed that AC treatment caused significant mitochondrial shrinkage, elevated mitochondrial membrane density, and decreased number of or no cristae (Fig. 4E,F).
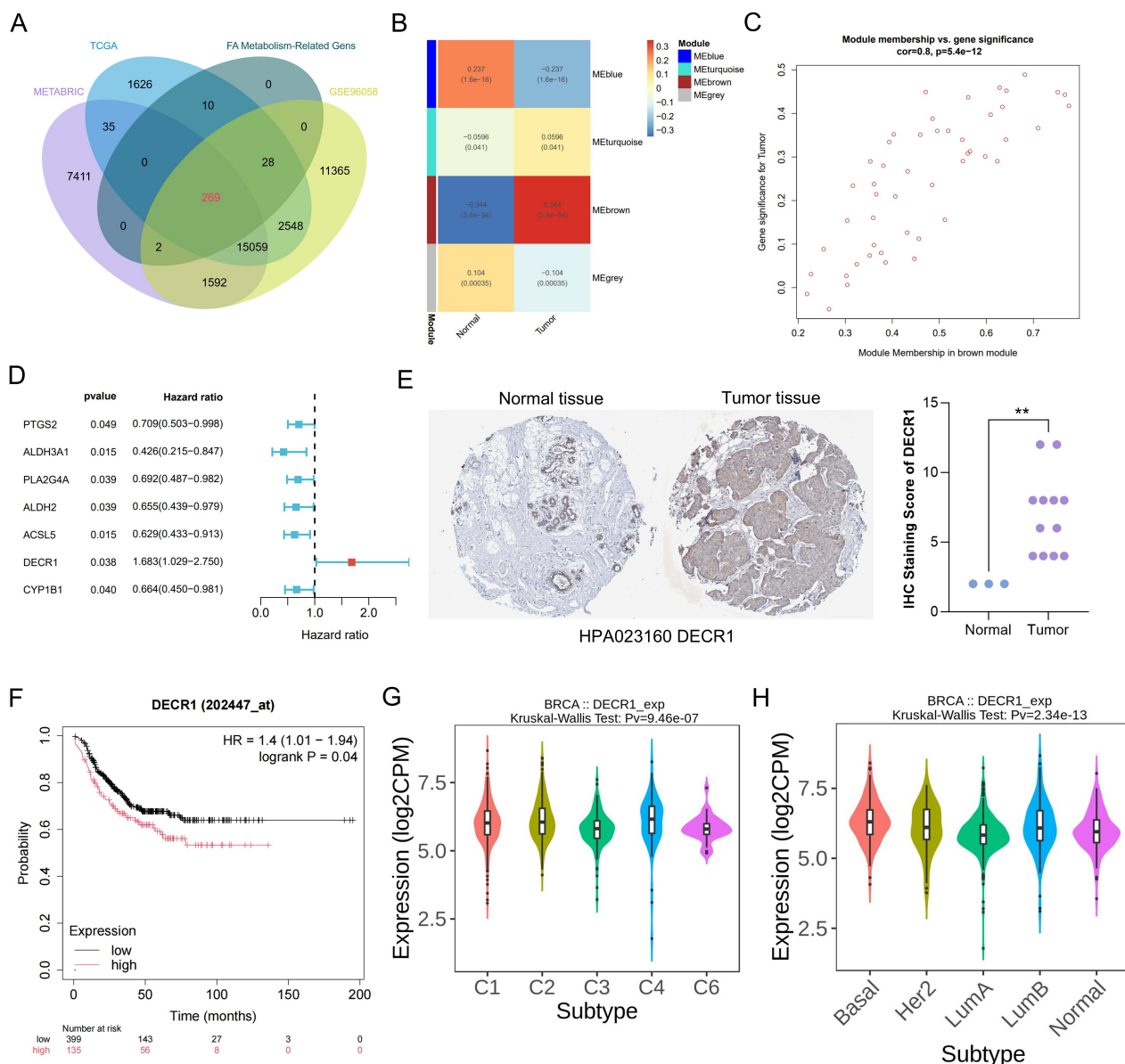
Fig. 1. DECR1 has potential as a candidate anti-BC target. (A) Identification of 269 reliable genes related to fatty acid metabolism, with a Venn diagram showing these 269 overlapping FMGs from the TCGA-BRCA, METABRIC, and GSE96058 datasets. (B) Characteristic gene adjacency heatmaps of the correlations between normal breast and tumor tissue module genes. (C) Correlations of gene significance with the module membership of the brown module with the highest absolute R-value. (D) Univariate Cox analysis conducted for screening the prognostic genes in the brown module. (E) Representative IHC staining of DECR1 in normal and tumor breast tissues from the Human Protein Atlas (HPA), along with semi-quantitative scoring of staining intensity. (F) Survival analysis for determining the correlation level of DECR1 expression in relation to patient outcomes (https://kmplot.com/). (G,H) TISIDB website findings showing significant relationships of DECR1 with immune subtypes and breast cancer subtypes. C1 to C6 denote the different immune subtypes. ** $p < 0.01$. FMGs, fatty acid metabolism-related genes; TCGA-BRCA, the Cancer Genome Atlas Breast Invasive Carcinoma dataset; METABRIC, Molecular Taxonomy of Breast Cancer International Consortium dataset; IHC, Immunohistochemistry staining; DECR1, 2,4-Dienoyl-CoA Reductase 1.

Intracellular lipid peroxides are important factors involved in the induction of ferroptosis. The detection of lipid peroxidation reflects the degree of ferroptosis in cells. In this study, markedly increased lipid peroxide content was noted in the AC treatment group (Fig. 5A). The accumulation of ROS (Fig. 5B) and Fe^{2+} (Fig. 5C) is a crucial factor in the occurrence of ferroptosis. This study revealed that the ROS and Fe^{2+} levels were significantly increased after AC treatment (Fig. 5D,E). Furthermore, ferroptosis inhibitors (ferrostatins) could effectively rescue tumor cells
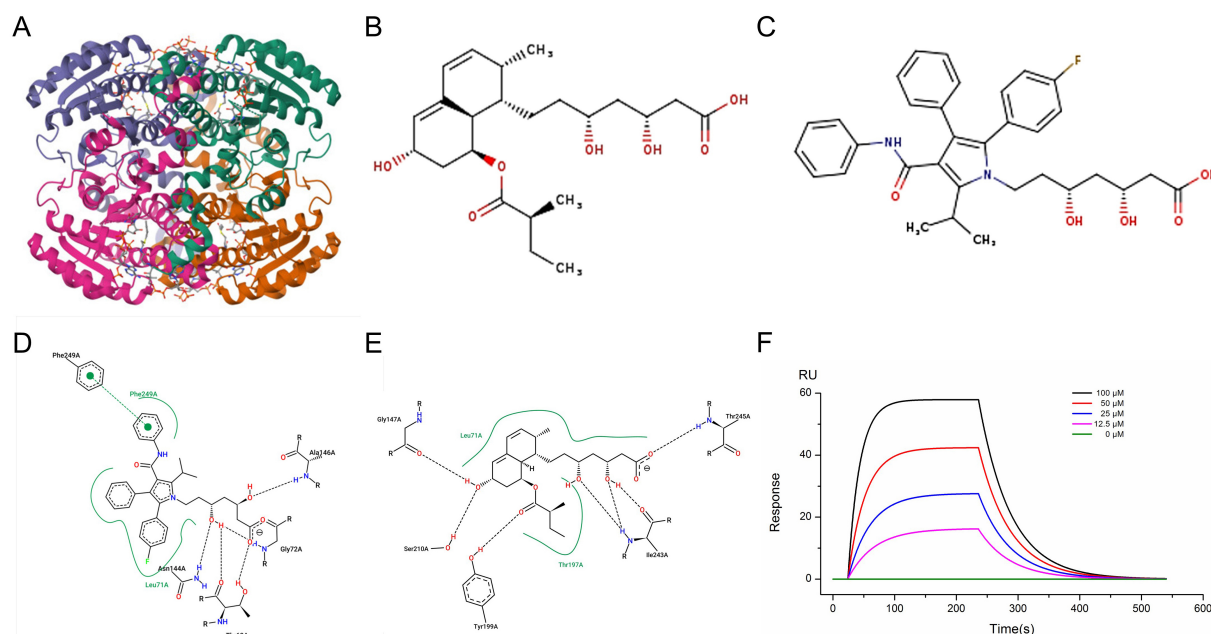
Fig. 2. Binding of DECR1 to pravastatin sodium and atorvastatin calcium. (A) The 3D structure of DECR1 (PDB ID: 1W6U). (B) Chemical structure of pravastatin sodium. (C) Chemical structure of atorvastatin. (D) Schematic for the molecular docking between pravastatin sodium and DECR1. (E) Molecular docking between atorvastatin calcium and DECR1. (F) Concentration gradient binding curve for the binding of DECR1 and atorvastatin calcium by SPR experiments and we confirmed the high affinity and specificity of AC binding to DECR1 *in vitro*. AC, atorvastatin calcium.

from death. In contrast, the combination of a ferroptosis inducer (erastin) with AC resulted in a synergistic effect that led to promoted breast cancer cell death (Fig. 6A,B). These results indicated that AC promotes BC cell ferroptosis.

3.5 Atorvastatin Calcium Exerts Antitumor Effects Associated With the DECR1-ACSL4 Axis

In order to explore the specific molecular mechanisms underlying AC-induced ferroptosis in breast cancer cells, the expressions of ferroptosis-related genes were determined in this study. Compared to those in the control group, the expressions of GPX4 and SLC7A11 in the AC treatment group were markedly decreased (Fig. 6C,D), which was consistent with previously reported findings [17,18]. Additionally, the expression of ACSL4 was obviously up-regulated in this study. At the protein level, the expression of ACSL4 was negatively correlated to that of DECR1 (Fig. 6E,F). AC inhibits DECR1 expression but promotes ACSL4 expression. Therefore, it was understood that AC not only induces ferroptosis by reducing the biosynthesis of GPX4 but may also promote ferroptosis by activating ACSL4 expression.

4. Discussion

Metabolic reprogramming typically involves alterations in energy metabolism, lipid metabolism, and amino acid metabolism, and is a common characteristic of tumors [19]. Researchers have long recognized the importance of glucose in tumor progression. However, changes in lipid metabolism also exert important effects on tumor growth, invasion, metastasis, and immune escape [20–22]. Tumor cells require increased *de novo* fatty acid synthesis to meet the demands of rapid membrane generation, energy production, and signal molecule transmission [23]. Cholesterol metabolism is critical to cancer progression, as altered cholesterol levels impact the fluidity of cell membranes, signaling pathways, and tumor growth [24]. Disruptions in cholesterol homeostasis have significant implications for tumor development and resistance to therapies [25].

Statins are strong competitive inhibitors of HMG-CoA reductase, and previous research has demonstrated their importance in the regulation of *de novo* cholesterol synthesis [26]. Statins mainly function to decrease the levels of circulating lipids, which can bind to HMG-CoA reductase while preventing the conversion of HMG-CoA into mevalonate, thus decreasing the intracellular cholesterol concentration. Statins have been evaluated for their potential in treating tumors from several perspectives. First, statins reduce the levels of low-density lipoprotein and affect cholesterol synthesis. Cholesterol, in significant amounts, serves as the raw material for the synthesis of membranes in rapidly dividing tumor cells. Second, statins decrease the production of proinflammatory factors [27]. Although there is little correlation between the use of statins and BC incidence, clinical evidence suggests that statins can reduce disease recurrence [28]. Moreover, statins could significantly reduce the risk of breast cancer-specific mortality (BCSM) in BC patients [29].
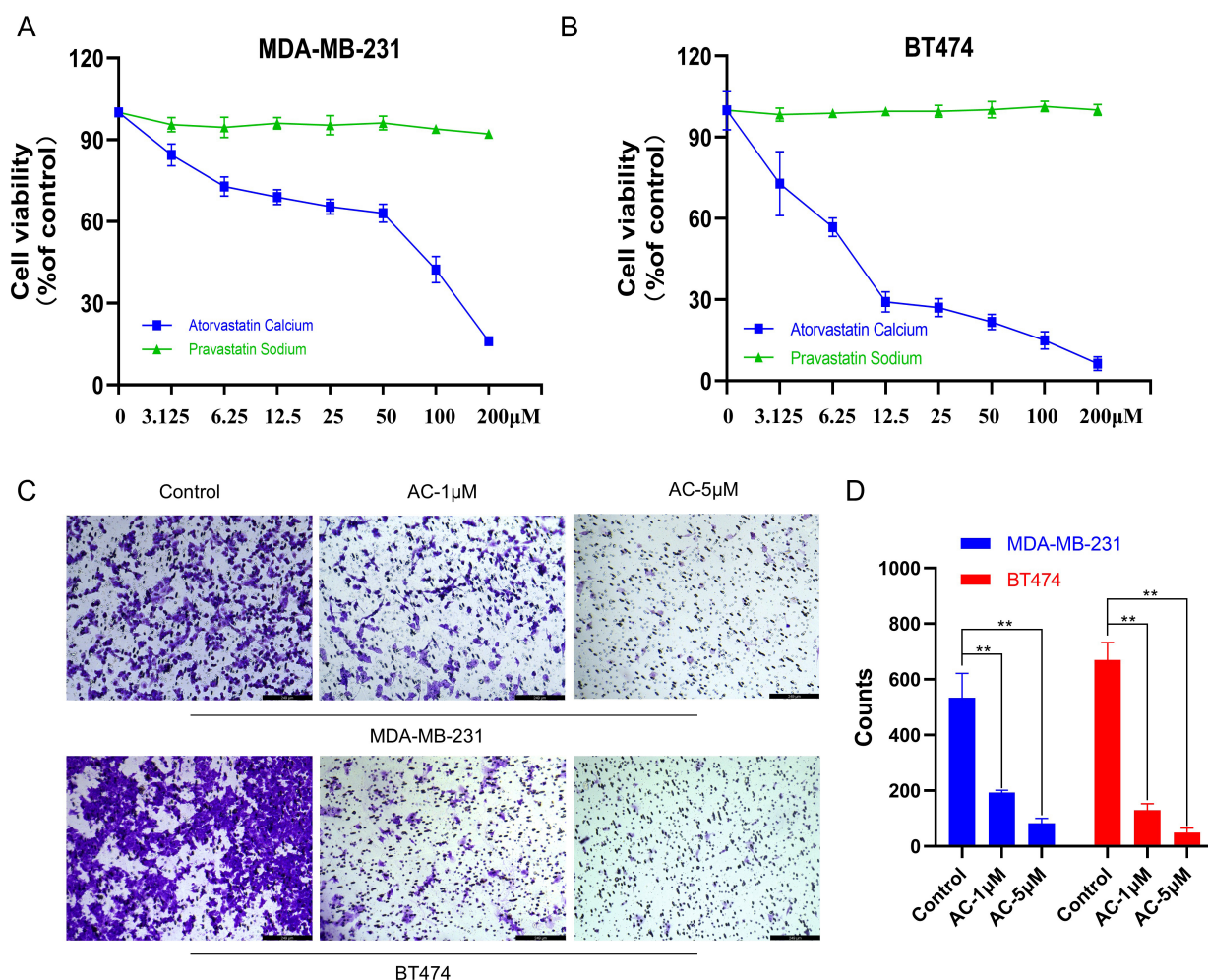
Fig. 3. Atorvastatin calcium (AC) has antitumor effects. (A,B) Compared to pravastatin sodium, AC markedly suppressed MDA-MB-231 (A) and BT474 (B) cell proliferation, with IC_{50} values of 39.70 µM and 7.74 µM, respectively. (C,D) AC treatment inhibits cell migration in breast cancer cells. (C) Representative images of migrated MDA-MB-231 and BT474 cells treated with AC at 1 µM and 5 µM, as assessed by Transwell migration assay, scale bar = 249 µm. (D) Quantification of migrated cells from (C). ** $p < 0.01$.

A previous study showed that statins downregulate glutathione peroxidase 4 (GPX4) through the suppression of HMG CoA reductase. GPX4 is a key regulatory factor for lipid peroxidation and can mediate the production of lipid ROS and induce ferroptosis in cells [30]. Atorvastatin reportedly induced mitochondria-dependent ferroptosis by regulating the Nuclear factor erythroid 2–related factor 2 (Nrf2)-GPX4 axis in human cardiomyocytes and mouse skeletal muscle cells [17]. A existing study on breast cancer have included simvastatin-induced ferroptosis as a potential therapeutic strategy against triple-negative breast cancer [7]. Pivastatin induces autophagy-dependent ferroptosis in breast cancer cells through the mevalonate pathway [31]. In addition to the mevalonate pathway, other possible pathways through which statins induce ferroptosis have not been elucidated to date in breast cancer, and the potential of atorvastatin calcium for breast cancer treatment remains to be fully understood. Therefore, DECR1 could serve as a viable target for breast cancer therapy, and AC, through its ability

to induce ferroptosis, represents a promising candidate for further development as a therapeutic tool. Research into the underlying mechanisms revealed that DECR1 inhibited the expression of ACSL4, thereby interfering with ferroptosis. DECR1 is a rate-limiting mitochondrial enzyme involved in the β-oxidation of PUFAs, playing a pivotal role in maintaining lipid homeostasis and regulating ferroptosis. A Previous study have demonstrated that DECR1 is highly expressed in prostate cancer, and its suppression leads to PUFA accumulation, increased lipid peroxidation, and elevated mitochondrial oxidative stress, ultimately triggering ferroptosis [32]. In our study, treatment with AC downregulated DECR1 expression, which may promote lipid peroxidation by disrupting lipid metabolism and thereby induce ferroptosis in breast cancer cells. This mechanism appears to operate independently of the classical mevalonate-GPX4 axis and offers novel insight into how AC may induce ferroptosis through DECR1-mediated lipid remodeling. This study, while providing promising insights into the
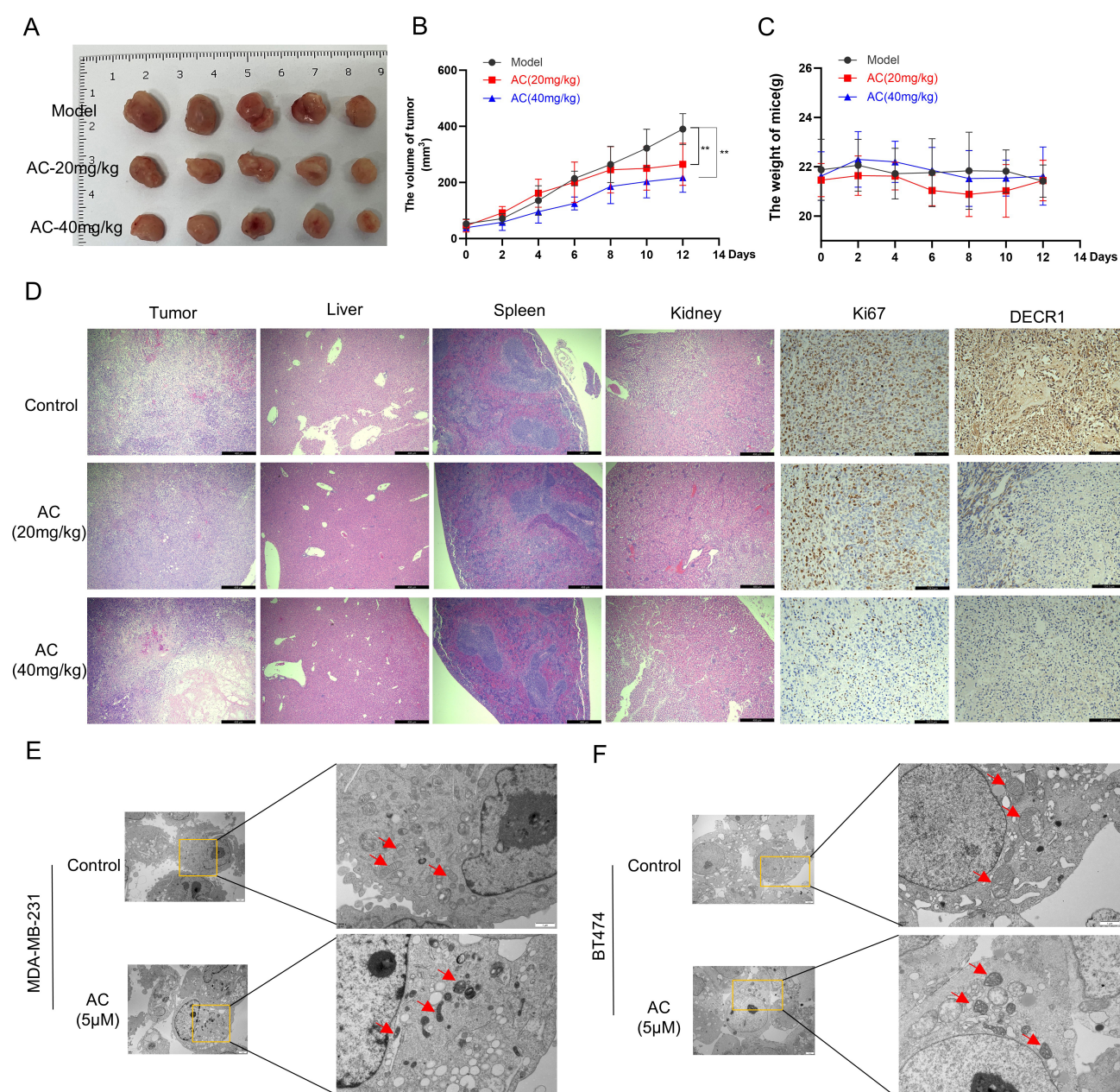
Fig. 4. The *in vivo* antitumor effects of AC. (A) Intraperitoneal administration of AC (20 mg/kg or 40 mg/kg) significantly inhibited tumor growth in the 4T1 subcutaneous tumor model. (B) The tumor growth curves for different treatment groups. (C) Mouse body weight changes during drug treatment. (D) HE staining of tumor, liver, spleen, and kidney tissues (scale bar = 498 μm) showed no significant morphological changes in the liver, kidney, or spleen following AC treatment. Immunohistochemical staining of Ki67 and DECR1 in tumor tissues (scale bar = 124.5 μm) revealed a marked decrease in expression, indicating suppressed cell proliferation and DECR1 expression after treatment. (E,F) Transmission electron microscopy revealed abnormal inner mitochondrial membrane structures in AC-treated MDA-MB-231 (E) and BT474 (F) cells, which are the typical features of ferroptosis. In each panel, the left image shows the overall cellular morphology (scale bar = 2 μm), while the right image displays a magnified view of the yellow-boxed region, highlighting mitochondrial damage (scale bar = 1 μm). Red arrows indicate condensed and ruptured mitochondrial cristae, characteristic of ferroptotic morphology. ** $p < 0.01$. HE, hematoxylin-eosin.

role of DECR1 and AC in breast cancer therapy, has, however, certain limitations that need to be considered. The present study was conducted primarily using *in vitro* models and subcutaneous tumor models, which may not fully replicate the complexities of human tumors. This necessitates further validation of the findings of this study in clinical trials and *in vivo* models. In addition, the precise molecular mechanisms through which AC induces ferrop-
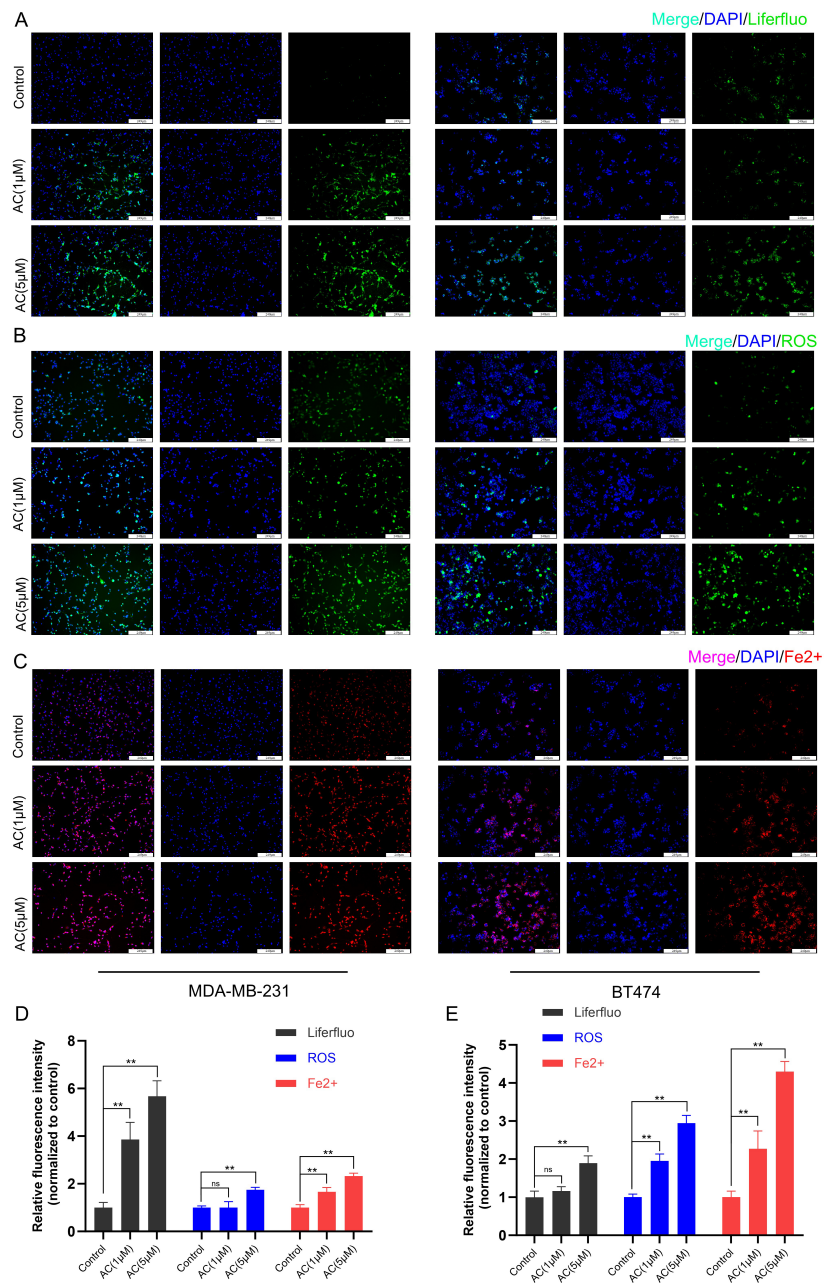
Fig. 5. Detection of ferroptosis-related markers in breast cancer cells after AC treatment. (A) Immunofluorescence analysis results revealed markedly elevated lipid peroxidation levels in AC-treated breast cancer cells compared to those in control cells. (B) ROS levels were significantly elevated following AC treatment. (C) The intracellular Fe^{2+} content also markedly increased after AC treatment. (D,E) Relative fluorescence intensity (normalized to control) in MDA-MB-231 (D) and BT474 cells (E). Fluorescence intensity values were normalized to the control group. The scale bars represent 249 μm in all images. ** $p < 0.01$, ns, not significant.

tosis and interacts with DECR1 remain unclear. For example, the precise mechanism through which DECR1 influences the expression of ACSL4 requires further investigation. Although our study demonstrates that AC induces ferroptosis through DECR1 inhibition, other ferroptosis-related pathways such as lipid remodeling (e.g., LPCAT3), oxidative stress responses (e.g., Nrf2/HO-1, FSP1), and iron metabolism (e.g., TFRC, ferritin) were not fully explored. Further investigation is warranted to delineate the broader landscape of ferroptosis regulation by AC in breast cancer. It is important to address these limitations for a better translation of the obtained results into effective clinical treatments.

5. Conclusions

This study integrated bioinformatics analysis, molecular docking, cell-based assays, and animal models to investigate the potential role of DECR1 in breast cancer
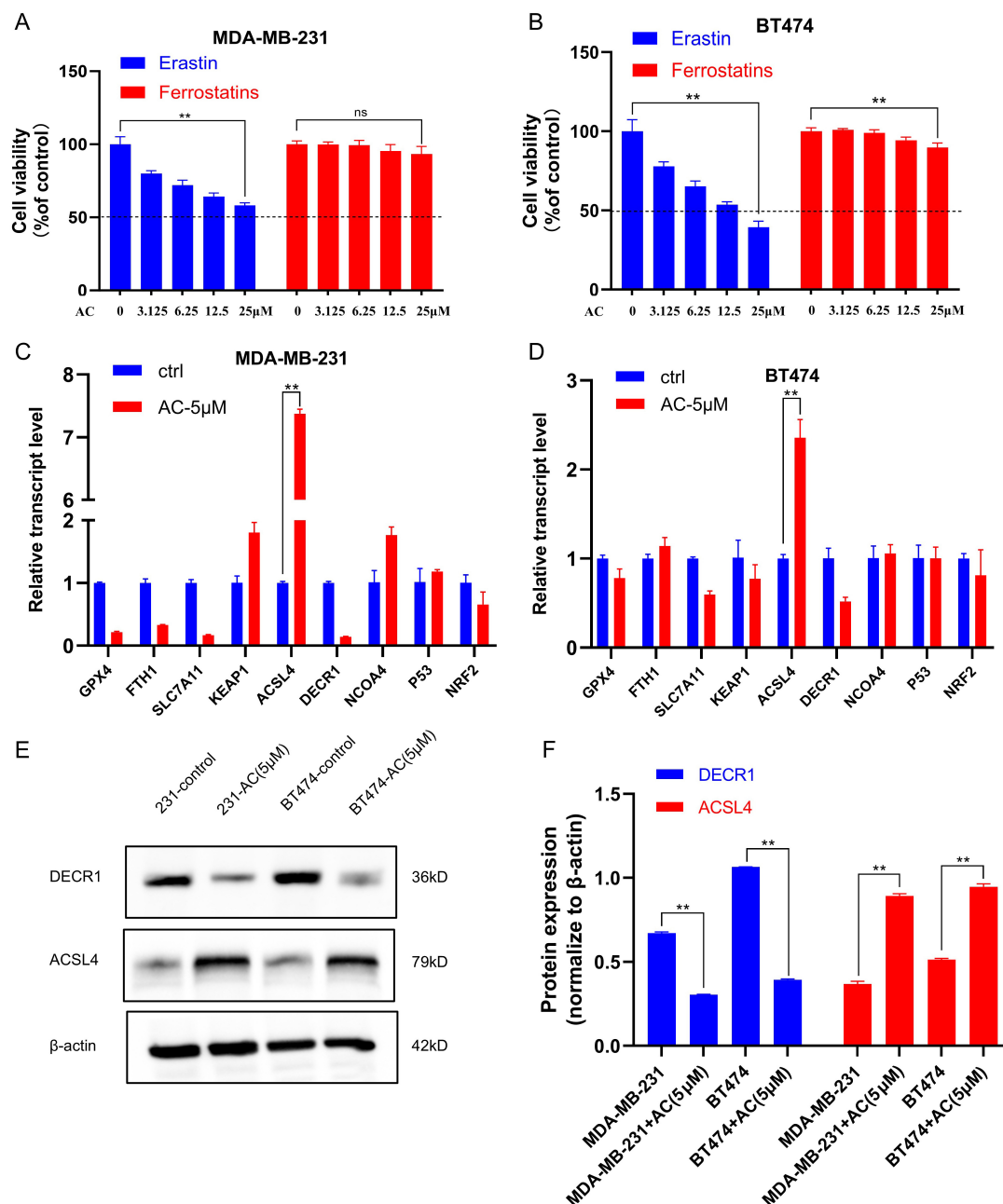
Fig. 6. Investigation of related mechanisms. (A,B) Cotreatment of MDA-MB-231 (A) and BT474 (B) cells with ferroptosis inducers (erastin, 10 µM), ferroptosis inhibitors (ferrostatins, 10 µM), and AC for 48 h. (C,D) qRT-PCR analysis of ferroptosis-related gene expression in MDA-MB-231 (C) and BT474 (D) cells treated with AC (5 µM) for 24 h. Notably, ACSL4 mRNA expression was significantly upregulated in both cell lines ($p < 0.01$), with a ~7.5-fold increase in MDA-MB-231 cells and a ~2.5-fold increase in BT474 cells. Expression levels of GPX4 and SLC7A11 showed moderate downregulation but did not reach statistical significance. Error bars represent SEM from three independent experiments. (E) Western blot analysis of DECR1 and ACSL4 protein expression in control and AC-treated MDA-MB-231 and BT474 cells. (F) Quantification of protein expression from (E), normalized to β-actin. AC treatment significantly decreased DECR1 expression and increased ACSL4 expression in both cell lines. ** $p < 0.01$, ns, not significant. AC, atorvastatin calcium; DECR1, 2,4-Dienoyl-CoA Reductase 1; ACSL4, Acyl-CoA Synthetase Long-Chain Family Member 4.

and explore the mechanism of action of AC. Our findings suggest that DECR1 plays a critical role in breast cancer progression, and that AC may exert its antitumor effects by modulating ferroptosis-related pathways involving DECR1. Overexpression of DECR1 is closely associated with poor prognosis in breast cancer patients, while AC treatment led to downregulation of DECR1 and upregulation of ACSL4, contributing to the induction of ferroptosis

in tumor cells. Furthermore, AC exhibited significant anti-tumor activity both *in vitro* and *in vivo*, with minimal toxicity to major organs. These results highlight DECR1 as a potential therapeutic target and support the further evaluation of AC as a candidate agent for breast cancer therapy. Future studies will aim to validate the direct role of DECR1 in mediating the antitumor effects of AC and to further elucidate its clinical translational potential.

Availability of Data and Materials

All data that support the findings of this study are included in this published article. Raw data are available from the corresponding author upon reasonable request.

Author Contributions

YL, HW and FZ designed this study; YL, HC and ZY performed all the experiment; ZY, YH analyzed and interpreted the data; YL, HC drafted the manuscript; YL, HW and FZ revised the manuscript. All authors contributed to editorial changes in the manuscript. All the authors read and approved the final manuscript. All authors have participated sufficiently in the work and agreed to be accountable for all aspects of the work.

Ethics Approval and Consent to Participate

The surgical procedures involving experimental animals were conducted with the approval of the Southwest University Animal Protection and Use Committee (No. LAC2025-1-0128). All experiments were carried out in accordance with relevant ethical regulations, including the 3Rs principle (Replacement, Reduction, and Refinement) and the ARRIVE guidelines. Every effort was made to minimize animal suffering and to ensure humane treatment throughout the study.

Acknowledgment

Funding

Conflict of Interest

The authors declare no conflict of interest.

Supplementary Material

Supplementary material associated with this article can be found, in the online version, at https://doi.org/10.31083/FBL38924.

References

[1] Zhou S, Liu J, Wan A, Zhang Y, Qi X. Epigenetic regulation of diverse cell death modalities in cancer: a focus on pyroptosis, ferroptosis, cuproptosis, and disulfidptosis. Journal of Hematology & Oncology. 2024; 17: 22. https://doi.org/10.1186/s13045-024-01545-6.

[2] Tan M, He Y, Yi J, Chen J, Guo Q, Liao N, *et al*. WTAP Mediates NUPR1 Regulation of LCN2 Through m^{6}A Modification to Influence Ferroptosis, Thereby Promoting Breast Cancer Proliferation, Migration and Invasion. Biochemical Genetics. 2024; 62: 876–891. https://doi.org/10.1007/s10528-023-10423-8.

[3] Wang L, Zhu Y, Huang C, Pan Q, Wang J, Li H, *et al*. Targeting ferroptosis in cancer stem cells: A novel strategy to improve cancer treatment. Genes & Diseases. 2025; 101678. https://doi.org/10.1016/j.gendis.2025.101678.

[4] Malla R, Kundrapu DB, Bhamidipati P, Nagaraju GP, Muniraj N. Unleashing the Power of Yes-Associated Protein in Ferroptosis and Drug Resistance in Breast Cancer, with a Special Focus on Therapeutic Strategies. Cancers. 2023; 15: 5728. https://doi.org/10.3390/cancers15245728.

[5] Jiang W, Hu JW, He XR, Jin WL, He XY. Statins: a repurposed drug to fight cancer. Journal of Experimental & Clinical Cancer Research. 2021; 40: 241. https://doi.org/10.1186/s13046-021-02041-2.

[6] Gales L, Forsea L, Mitrea D, Stefanica I, Stanculescu I, Mitrica R, *et al*. Antidiabetics, Anthelmintics, Statins, and Beta-Blockers as Co-Adjuvant Drugs in Cancer Therapy. Medicina. 2022; 58: 1239. https://doi.org/10.3390/medicina58091239.

[7] Yao X, Xie R, Cao Y, Tang J, Men Y, Peng H, *et al*. Simvastatin induced ferroptosis for triple-negative breast cancer therapy. Journal of Nanobiotechnology. 2021; 19: 311. https://doi.org/10.1186/s12951-021-01058-1.

[8] O'Grady S, Crown J, Duffy MJ. Statins inhibit proliferation and induce apoptosis in triple-negative breast cancer cells. Medical Oncology. 2022; 39: 142. https://doi.org/10.1007/s12032-022-01733-9.

[9] Zhou Q, Meng Y, Li D, Yao L, Le J, Liu Y, *et al*. Ferroptosis in cancer: From molecular mechanisms to therapeutic strategies. Signal Transduction and Targeted Therapy. 2024; 9: 55. https://doi.org/10.1038/s41392-024-01769-5.

[10] Zhang S, Chang W, Wu H, Wang YH, Gong YW, Zhao YL, *et al*. Pan-cancer analysis of iron metabolic landscape across the Cancer Genome Atlas. Journal of Cellular Physiology. 2020; 235: 1013–1024. https://doi.org/10.1002/jcp.29017.

[11] Liberzon A, Birger C, Thorvaldsdóttir H, Ghandi M, Mesirov JP, Tamayo P. The Molecular Signatures Database (MSigDB) hallmark gene set collection. Cell Systems. 2015; 1: 417–425. https://doi.org/10.1016/j.cels.2015.12.004.

[12] Langfelder P, Horvath S. WGCNA: an R package for weighted correlation network analysis. BMC Bioinformatics. 2008; 9: 559. https://doi.org/10.1186/1471-2105-9-559.

[13] Ru B, Wong CN, Tong Y, Zhong JY, Zhong SSW, Wu WC, *et al*. TISIDB: an integrated repository portal for tumor-immune system interactions. Bioinformatics. 2019; 35: 4200–4202. https://doi.org/10.1093/bioinformatics/btz210.

[14] Thorsson V, Gibbs DL, Brown SD, Wolf D, Bortone DS, Ou Yang TH, et al. The Immune Landscape of Cancer. Immunity. 2018; 48: 812–830.e14. https://doi.org/10.1016/j.immuni.2018.03.023.

[15] Bugnon M, Röhrig UF, Goullieux M, Perez MAS, Daina A, Michielin O, *et al*. SwissDock 2024: major enhancements for small-molecule docking with Attracting Cavities and AutoDock Vina. Nucleic Acids Research. 2024; 52: W324–W332. https://doi.org/10.1093/nar/gkae300.

[16] Eberhardt J, Santos-Martins D, Tillack AF, Forli S. AutoDock Vina 1.2.0: New Docking Methods, Expanded Force Field, and Python Bindings. Journal of Chemical Information and Modeling. 2021; 61: 3891–3898. https://doi.org/10.1021/acs.jcim.1c00203.

[17] Zhang Q, Qu H, Chen Y, Luo X, Chen C, Xiao B, *et al*. Atorvastatin Induces Mitochondria-Dependent Ferroptosis *via* the Modulation of Nrf2-xCT/GPx4 Axis. Frontiers in Cell and Developmental Biology. 2022; 10: 806081. https://doi.org/10.3389/fcell.2022.806081.

[18] Liu T, Shu J, Liu Y, Xie J, Li T, Li H, *et al*. Atorvastatin attenuates ferroptosis-dependent myocardial injury and inflammation following coronary microembolization *via* the Hif1a/Ptgs2 pathway. Frontiers in Pharmacology. 2022; 13: 1057583. https://doi.org/10.3389/fphar.2022.1057583.

[19] Faubert B, Solmonson A, DeBerardinis RJ. Metabolic reprogramming and cancer progression. Science. 2020; 368: eaaw5473. https://doi.org/10.1126/science.aaw5473.

[20] Cheng C, Geng F, Cheng X, Guo D. Lipid metabolism reprogramming and its potential targets in cancer. Cancer Communications. 2018; 38: 27. https://doi.org/10.1186/s40880-018-0301-4.

[21] Zhu L, Zhu X, Wu Y. Effects of Glucose Metabolism, Lipid Metabolism, and Glutamine Metabolism on Tumor Microenvironment and Clinical Implications. Biomolecules. 2022; 12: 580. https://doi.org/10.3390/biom12040580.

[22] He M, Xu S, Yan F, Ruan J, Zhang X. Fatty Acid Metabolism: A New Perspective in Breast Cancer Precision Therapy. Frontiers in Bioscience (Landmark Edition). 2023; 28: 348. https://doi.org/10.31083/j.fbl2812348.

[23] Zipinotti Dos Santos D, de Souza JC, Pimenta TM, da Silva Martins B, Junior RSR, Butzene SMS, *et al*. The impact of lipid metabolism on breast cancer: a review about its role in tumorigenesis and immune escape. Cell Communication and Signaling. 2023; 21: 161. https://doi.org/10.1186/s12964-023-01178-1.

[24] Kuzu OF, Noory MA, Robertson GP. The Role of Cholesterol in Cancer. Cancer Research. 2016; 76: 2063–2070. https://doi.org/10.1158/0008-5472.CAN-15-2613.

[25] Delmas D, Mialhe A, Cotte AK, Connat JL, Bouyer F, Hermetet F, *et al*. Lipid metabolism in cancer: Exploring phospholipids as potential biomarkers. Biomedicine & Pharmacotherapy = Biomedecine & Pharmacotherapie. 2025; 187: 118095. https://doi.org/10.1016/j.biopha.2025.118095.

[26] Coradini D. *De novo* cholesterol biosynthesis: an additional therapeutic target for the treatment of postmenopausal breast cancer with excessive adipose tissue. Exploration of Targeted Anti-Tumor Therapy. 2022; 3: 841–852. https://doi.org/10.37349/etat.2022.00116.

[27] Xu X, Gao W, Cheng S, Yin D, Li F, Wu Y, *et al*. Anti-inflammatory and immunomodulatory mechanisms of atorvastatin in a murine model of traumatic brain injury. Journal of Neuroinflammation. 2017; 14: 167. https://doi.org/10.1186/s12974-017-0934-2.

[28] Ahern TP, Lash TL, Damkier P, Christiansen PM, Cronin-Fenton DP. Statins and breast cancer prognosis: evidence and opportunities. The Lancet. Oncology. 2014; 15: e461–8. https://doi.org/10.1016/S1470-2045(14)70119-6.

[29] Beckwitt CH, Brufsky A, Oltvai ZN, Wells A. Statin drugs to reduce breast cancer recurrence and mortality. Breast Cancer Research. 2018; 20: 144. https://doi.org/10.1186/s13058-018-1066-z.

[30] Sahebkar A, Foroutan Z, Katsiki N, Jamialahmadi T, Mantzoros CS. Ferroptosis, a new pathogenetic mechanism in cardiometabolic diseases and cancer: Is there a role for statin therapy? Metabolism. 2023; 146: 155659. https://doi.org/10.1016/j.metabol.2023.155659.

[31] Tang WJ, Xu D, Liang MX, Wo GQ, Chen WQ, Tang JH, *et al*. Pitavastatin induces autophagy-dependent ferroptosis in MDA-MB-231 cells via the mevalonate pathway. Heliyon. 2024; 10: e27084. https://doi.org/10.1016/j.heliyon.2024.e27084.

[32] Nassar ZD, Mah CY, Dehairs J, Burvenich IJ, Irani S, Centenera MM, *et al*. Human DECR1 is an androgen-repressed survival factor that regulates PUFA oxidation to protect prostate tumor cells from ferroptosis. eLife. 2020; 9: e54166. https://doi.org/10.7554/eLife.54166.